FUDMA Journal of Sciences (FJS)
ISSN online: 2616-1370
ISSN print: 2645 - 2944
Vol. 5 No. 1, March, 2021, pp 347 – 357
DOI: https://doi.org/10.33003/fjs-2021-0501-575

A TIME DEPENDENT STUDY FOR THE FORMATION OF ULTRASMALL Cs-AlMCM-41 HOLLOW NANOSPHERES

\

***Haruna Abdullahi, Sadiq Sani and Kamaluddeen S. Kabo**

Department of Chemistry, Federal University Dutsin-Ma

*Corresponding author's email: abharun01@yahoo.com

ABSTRACT

Monitoring of the formation of ultrasmall Cs-AlMCM-41 nanospheres under hydrothermal condition has been performed. It showed that when the CTABr surfactant, silica and alumina were mixed, homogenization of raw materials was first taking place, where CTABr molecules first interacted with the inorganic species *via* self-assembly into helical rod-like micelles. Hydrolysis, condensation and polymerization of silica and alumina precursors were then initiated. In addition, the Cs^+ cation also participated during the formation of MCM-41 structure where it counterbalanced the negative charge of the aluminosilicate surface. After 14 h, the aluminosilicate oligomers were produced and fully enclosed the spherical micelles. Further increasing the hydrothermal treatment to 24 h onwards, polycondensation silanol siloxane would take place leading to the emergence of well-defined and highly ordered MCM-41 structure. This study came up with a clear picture on the formation of Cs-AlMCM-41 hollow nanospheres in cationic-surfactant-templated. This suggested that similar studies for other mesoporous materials such as MCM-48 and MCM-50 under different conditions and approaches could also be explored.

Keywords: ultrasmall, nanoparticle, mesoporous, aluminosilicate, surfactant**.**

INTRODUCTION

Mesoporous materials are an important class of porous solids having pore sizes from 2 to 50 nm (Kresge *et al*. 1992). Since the first discovery of MCM-41 in 1992, a number of patents and publications on the synthesis of this mesomaterial and other new mesoporous silica (e.g. SBA, FDU, FSM, HMS, and MSU) have been reported. The chemical interaction and self-assembly mechanism between the surfactants and inorganic precursors have been discussed (Inagaki et al., 1993; Tanev and Pinnavaia, 1995; Bagshaw et.al 1995; Zhao et al., 1998; Liu *et al* 2002).

Typically, the MCM-41 mesoporous materials are synthesized in 2-dimensional structure (Bagshaw et.al 19950. Recently, the preparation of nanosized MCM-41 is receiving intensive attention due to their unique properties which are not found in conventional MCM-41 solids (Naraya and Nayak, 2018; Maiti *et al.,* 2016). The synthesis of ultrasmall MCM-41 nanoparticles is highly demanded for advanced applications, especially in biomedical and catalysis fields. However, the detailed evolution of MCM-41 nanoparticles containing Al and Cs elements have not been reported so far. In this chapter, the evolutional formation of ultrasmall Cs-AlMCM-41 hollow nanospheres was reported which was investigated by complementary analyses involving advanced characterization techniques such as XRD, TEM, FTIR, N_2 sorption, TGA/DTG and XRF. The study was performed by interrupting the formation at various intervals and the solids were systematically characterized until well-ordered ultrasamall Cs-AlMCM-41 hollow nanospheres was formed.

MATERIALS AND METHODS

Materials

Cesium hydroxide monohydrate ($CsOH{\cdot}H_2O$, ≥99.5%), Ludox AS-40 (40%), aluminum isopropoxide (98%), acetic acid (CH_3COOH, ≥99.7%), were purchased from Sigma-Aldrich GmbH, while cetyltrimethylammonium bromide (CTABr, 97%) was purchased from Merck Chemicals GmbH. All chemicals were used without additional purification

METHODS

Ultrasmall CsMCM-41 with hollow nanospheres (CsM-30) with a SiO_2/Al_2O_3 ratio = 30 were synthesized as follows: Clear Solution 1 was first prepared by dissolving CTABr

(4.388 g, 97%) into distilled water (80.742 g). Solution 2 was prepared by mixing $CsOH{\cdot}H_2O$ (3.963 g, 99.5%) and Ludox AS-40 (7.030 g, 40%). Solution 2 was then added into Solution 1 while stirring (400 rpm) before aluminum isopropoxide (0.210 g, 98%) was added into the mixture and the precursor with a final chemical composition of $4SiO_2$: $0.13Al_2O_3$: 1CTABr: $1Cs_2O$: $400H_2O$ was obtained. The stirring was stopped after 15 min, and the reaction mixture was hydrothermally treated at 100 °C. Samples were taken out at different time intervals (0 h, 10 h, 14 h and 24 h) throughout the hydrothermal process. The white solids were filtered, washed thoroughly with distilled water and dried at 60 ^oC overnight. These samples were denoted as M-0h, M-10h, M-14h, and M-24h (Liu *et al*,. 2013; and Ghear *et al.*, 2019).

Characterization

Powder X-ray diffraction (XRD) patterns were collected on a Bruker-AXS D8 diffractometer with Cu $K_\square$ radiation (λ = 1.5418 Å). Fourier-Transform Infrared (FT-IR) spectra were recorded with a Perkin Elmer's System 2000 FTIR spectrometer, using the KBr method (KBr: sample weight ratio = 200:1). Transmission electron microscopy (TEM) images were captured using a PHILIPS CM-12 TEM with an acceleration voltage of 200 kV. The chemical composition and the elemental mapping of the solids were obtained with an Oxford Instruments X-Max 80 mm^2 Solid State EDX detector which was equipped onto a JEOL JSM-6701F FESEM microscope. Thermogravimetric/differential thermal gravimetric analysis (TGA/DTG) was performed using a Mettler TGASDTA851 instrument at a heating rate of 20 °C min^{-1} under air flow. N_2 adsorption-desorption isotherms were measured at –196 °C on a Micromeritics ASAP 2010 instrument. The solid was degassed for 15 h at 300 °C before analysis. The chemical composition of the solids was also determined using a Philips PW2404 X-ray fluorescence spectrometer (XRF) (Ghear *et al.*, 2019).

RESULTS AND DISCUSSION

The progressive formation of Cs-AlMCM-41 was monitored by powder XRD instrument. No diffraction peak was observed at 0 h indicating that an amorphous sample with non-uniform structure was obtained (Figure 1a). After 10 h of heating at 100 ^0C reaction time, a weak diffraction peak at $2\theta = 2.23^0$ due to (100) plane started to appear (Naraya and Nayak, 2018). This suggested that the Cs-AlMCM-41 oligomers had started forming but were still not well developed (Figure 1b). As the synthesis time was extended to 14 h, the diffraction peak of (100) plane became more intense. In addition, three weak peaks at $2\theta = 3.86^0$, 4.50^0 and 5.94^0 due to (110), (200) and (210) planes started to appear (Naraya and Nayak, 2018). Thus, it showed that the degree of meso-ordering of the sample increased when the hydrothermal treatment was taking place (Kresge *et al.*, 1992). After the hydrothermal heating was extended to 24 h, the peak intensity of these four diffraction peaks increased explaining their uniform and ordered distribution of the channel diameters in the resulting products. Moreover, the XRD peaks was also slightly shifted to the higher angle (2.15^0 to 2.23^0) as the sample was heated from 10 h to 24 h. This indicated that the pore diameter of Cs-AlMCM-41 gradually decreased with hydrothermal time due to the formation of more rigid Si-O-T (T = Si or Al) bonds (Liu *et al*,. 2013). As a result, the progressive increase in unit cell parameter occurs (Table 1).

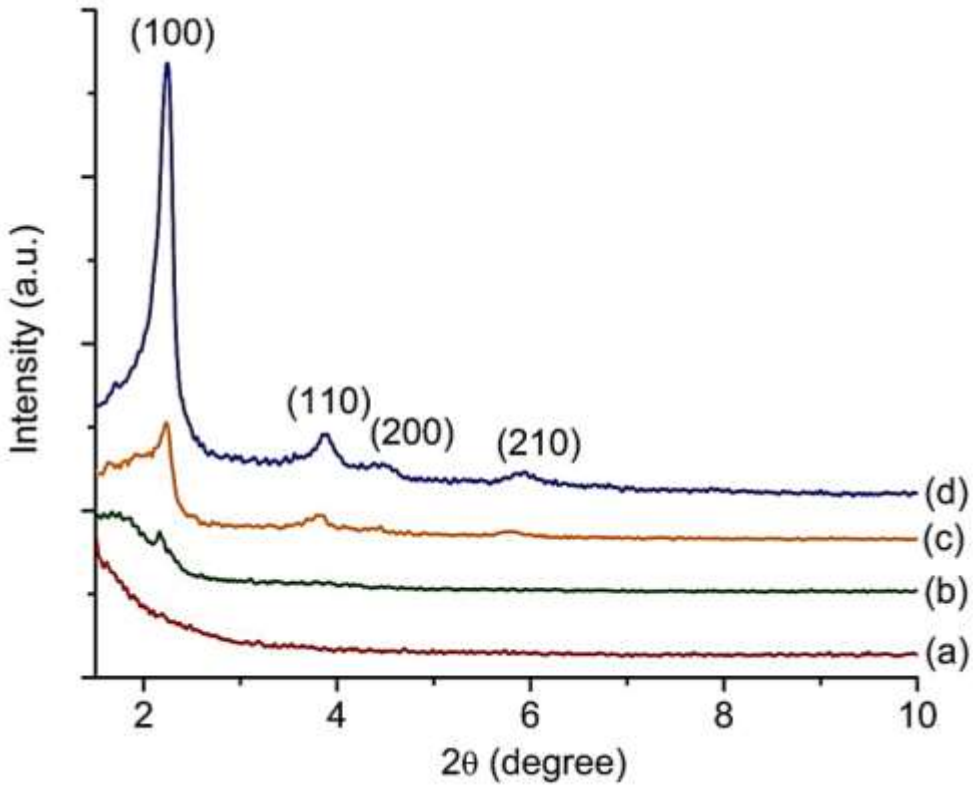

Figure 1. XRD patterns of solids after (a) 0 h, (b) 10 h, (c) 14 h and (d) 24 h of hydrothermal synthesis.

Table 1: Textural properties of the MCM-41 samples

Samples	d_{100} spacing (nm)	Unit cell, a_o (nm)[a]	Surface area, S_{BET} (m^2g^{-1})	Pore volume, V_{total} (cm^3g^{-1})	Pore diameter, D (Å)[b]
M-0h	NA	NA	122	0.520	0
M-10h	3.84	4.43	406	0.722	20.17
M-14h	3.96	4.57	468	0.828	19.78
M-24h	3.92	4.53	563	1.327	19.71

[a] $a_o = \frac{2d_{100}}{\sqrt{3}}$ (Jenkins, 2006)

[b] From BJH analysis

The TEM images of the samples heated for different times were shown in Figure 2. The initial sample (0 h) showed 3D irregular network where no specific shape could be identified (Figure 2a,b). This observation agreed with the XRD data (Figure 1a). When the heating time was extended to 10 h, the morphology of the sample changed significantly and nanospheres of ca. 34 nm embedded in bulk amorphous entities were seen (Figure 2c,d). These bulk amorphous entities, however, disappeared as the reaction time was extended to 14 h, leaving monodisperse nanospheres with reduced particle size (ca. 27 nm) (Figure 2e,f). As seen, the mesoporosity was hardly detected at this stage due to low meso-ordering as also revealed by XRD data (Figure 1c). The morphology of the Cs-AlMCM-41 solids gradually changed to nanospherical shape with hollow structure as the hydrothermal treatment was heated to 24 h (Figure 2g,h). According to the TEM image, uniform mesopores at the core surface and uniform shell thickness (ca. 6.0 nm) were seen on the nanospheres. Interestingly, the MCM-41 solid obtained in this work was different from those reported in the literature (Liu and Xu, 2019; Slowing *et al.*, 2006).

The solid product yield versus the heating time was also plotted in order to understand the formation of Cs-AlMCM-41 hollow nanospheres (Figure 4.3). At 0 h, 40% of solid was successfully recovered. The solid product yield increased to 57% after 10 h which could be due to the polycondensation of silica and alumina species. More solid product precipitated out as the hydrothermal heating period increased to 14 h and 24 h; 63% and 67% of yield were recorded, respectively.

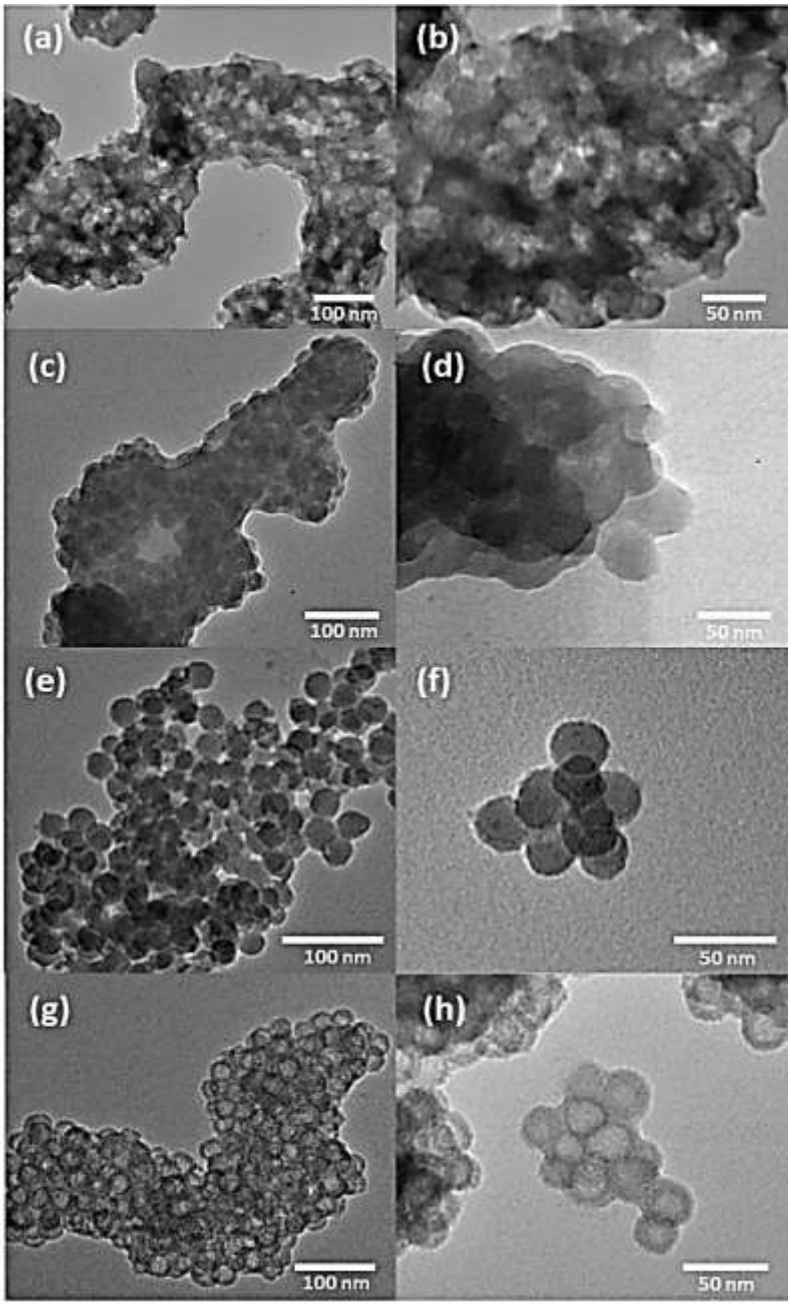

Figure 2. TEM images of Cs-AlMCM-41 solids after (a,b) M-0h, (c,d) M-10h, (e,f) M-14h and (g,h) M-24h of hydrothermal treatment.

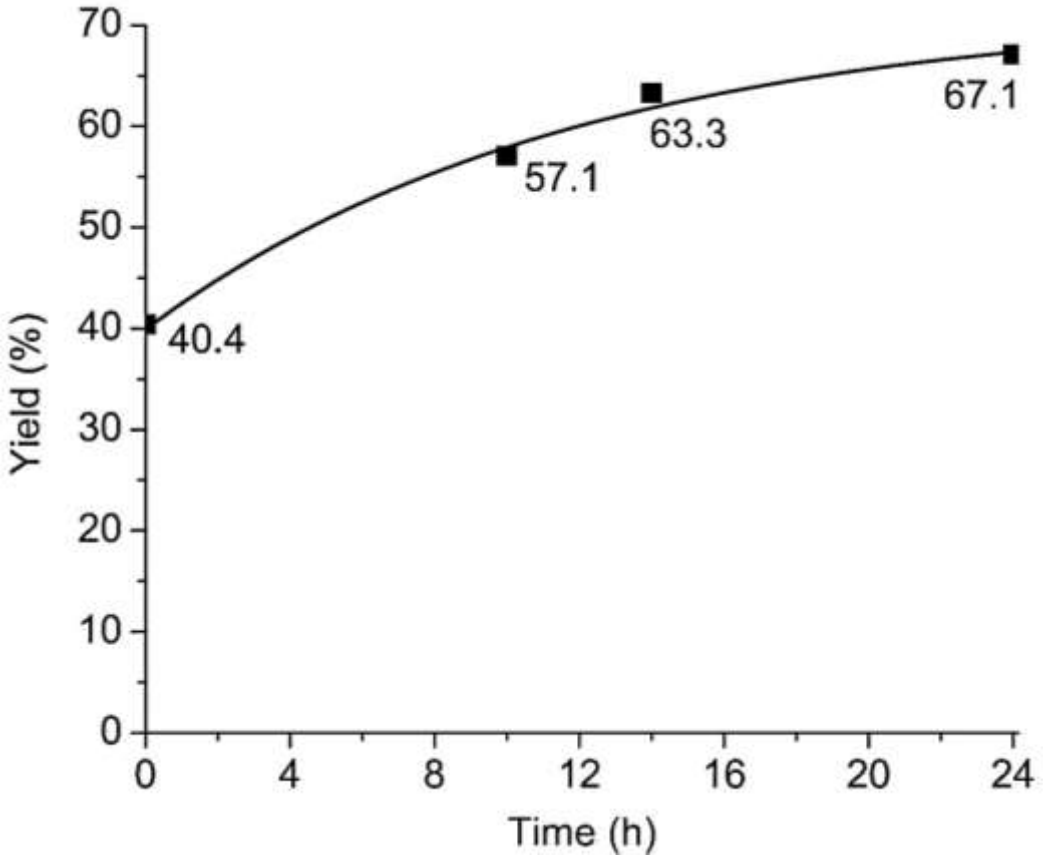

Figure 3. Yield of solids after (a) M-0h, (b) M-10h, (c) M-14h and (d) M-24h of hydrothermal heating.

The formation of Cs-AlMCM-41 was also studied by means of IR spectroscopy. For M-0h, the IR spectroscopy indicated that some CTABr surfactant molecules were occluded in the solid indicating the direct interaction between CTABr with the aluminosilicate oligomers (Figure 4a). It can be proven based on the presence of IR bands at 2928, 2858, 1463 and 800 cm^{-1} which were attributed to the presence of alkyl groups of CTABr (Franco and Oliveira, 2013). The IR bands at 3438 and 1640 cm^{-1} were attributed to the adsorbed moisture (HO–H group) (Rahman *et al.,* 2017). As seen, M-0h showed the least intense bands compared to the other three samples indicating that M-0h contained the lowest amount of occluded CTABr template.

Furthermore, the IR bands at 1223, 1091, 807 and 448 cm^{-1} could be respectively assigned to the asymmetric stretching, symmetric stretching and bending vibration of Si-O-T (T = Si or Al) (Figure 4a) (Ng *et al.,* 2006). The siloxane (Si-O-Si) oligomers were the basic units for the construction of the Cs-AlMCM-41 mesoporous structure. The bending mode of isolated silanol (Si-OH) was detected at 925 cm^{-1} (Petcu *et al.,* 2017). At 10 h, the peak intensity due to Si-O-Si and Si-OH functional groups was increasing (Figure 4b). However, no change in the peak intensity after 14 h occurred indicating that the completion of hydrolysis and polycondensation of aluminosilicate networks (Figure 4c). In addition, the bands at ca. 1220 and 1096 cm^{-1} were red shifted indicating that more Al atoms had been successfully isomorphous substituted into the MCM-41 mesoframework (Ng *et al.,* 2006).

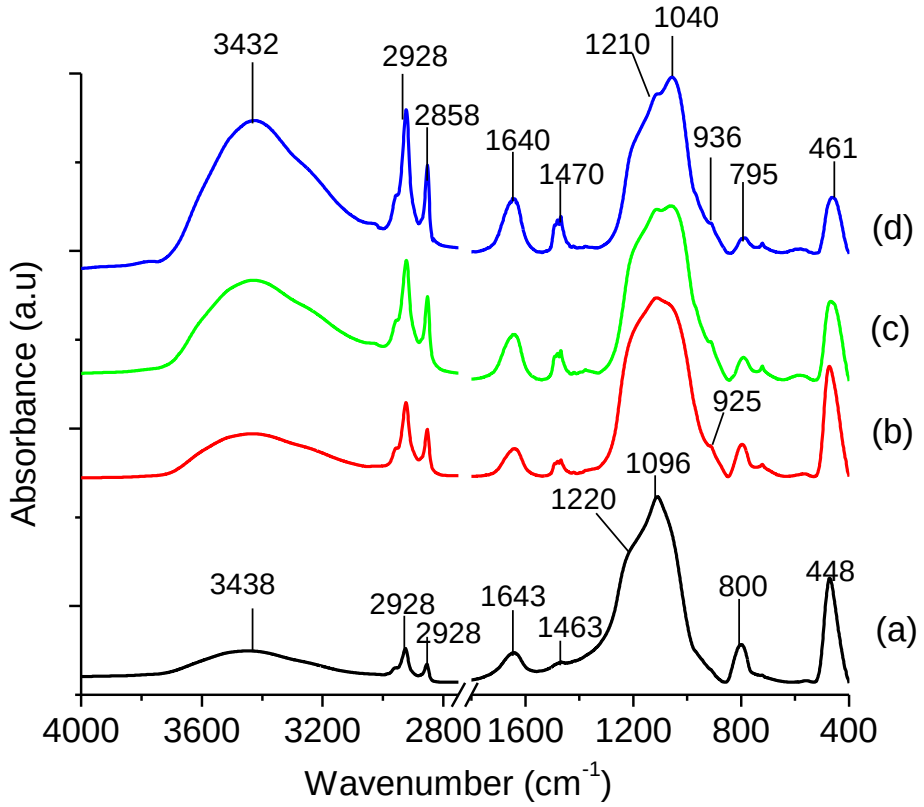

Figure 4. FTIR spectra of as-synthesized Cs-AlMCM-41 solids after (a) M-0h, (b) M-10h, (c) M-14h and (d) M-24h of hydrothermal treatment.

The IR spectroscopy analysis was further confirmed by TGA/DTG analysis (Figure 5 and 6). Three steps of weight loss were clearly observed by all samples. The first step of weight loss at below 135 ^{0}C was due to the removal of physisorbed water (Watanabe, 2018). The amount of water adsorbed increased with synthesis time which was in line with the IR spectroscopy data where M-0h released the least amount of physisorbed H_2O (2.39%) due to its low surface area (122 m^2g^{-1}) (Table 1). On the other hand, M-24h released the largest amount of physisorbed H_2O (ca. 5.75%) which is due to its well-defined mesoporous structure with larger surface area (563 m^2g^{-1}).

The second step of weight loss at 135-500 ^{0}C was attributed to the release of chemisorbed water and the decomposition of occluded template *via* Hofmann elimination (Aiube and Oliveira, 2019). The amount of occluded CTA^+ during the formation of MCM-41 framework increased with heating time. For M-0h, 10.09% of CTA^+ molecule decomposed, and it increased to 18.55% (M-10h), 33.24% (M-14h) and 44.82% (M-24h). Therefore, it indicated that M-0h and M-10h had a very low degree of mesostructured ordering due to insufficient amount of CTA^+ template (Braga *et al.*, 2011).

The third step of weight loss above 500 ^{0}C was due to the oxidation of the remaining organic components to carbon dioxide, water and probably residual carbonaceous species (Petcu *et al.*, 2017). At this step, small quantity of water was also produced from Si–OH condensation forming siloxane (Si–O–Si) group. M-0h recorded 1.47% loss at this stage due to the amorphous nature of framework and its weight loss was higher than the other three samples (M-10h: 1.67%, M-14h: 1.84%, M-24h: 2.38%).

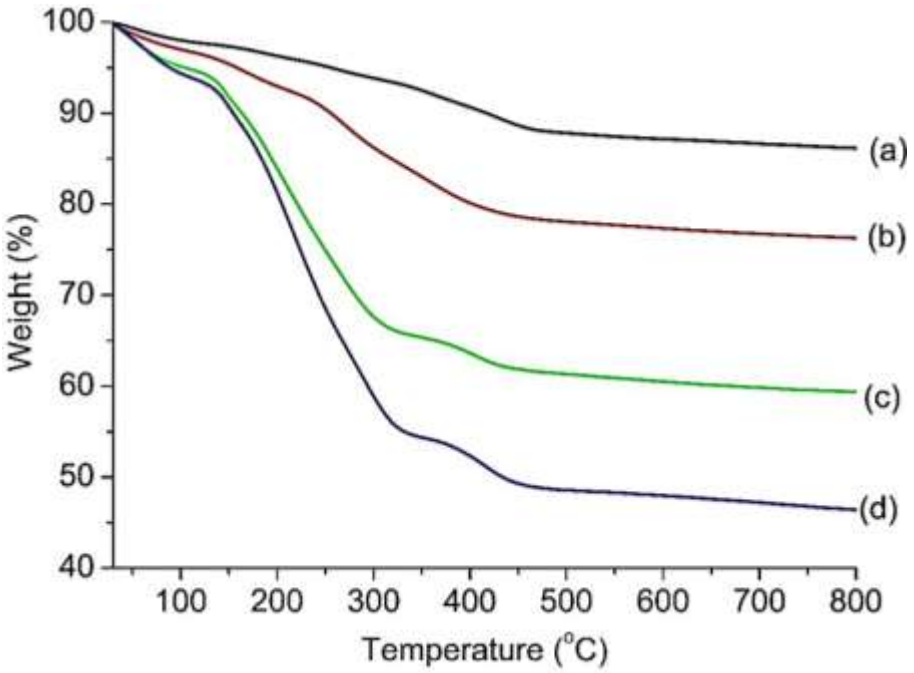

Figure 5. Thermograms of as-synthesized MCM-41 solids after (a) M-0h, (b) M-10h, (c) M-14h and (d) M-24h of hydrothermal treatment.

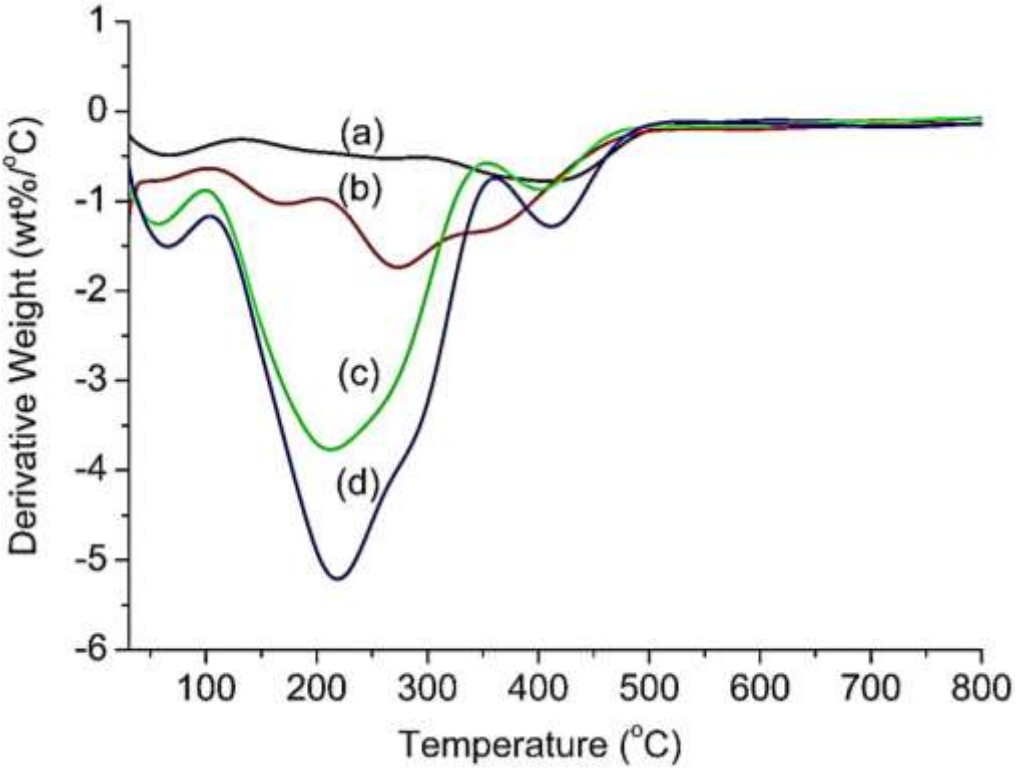

Figure 6. DTG curves of as-synthesized MCM-41 solids after (a) M-0h, (b) M-10 M-h, (c) M-14h and (d) M-24h of hydrothermal treatment.

The formation of Cs-AlMCM-41 hollow nanospheres was also studied by using N_2 adsorption-desorption isothermal analysis. Figure 7 showed the N_2 adsorption-desorption isotherms of the four calcined samples. M-0h displayed a typical type III isotherm revealing its macroporous/non-porous nature (Yildirim *et al.*, 2011). As seen from Table 4.1, M-0h had low surface area (122 m^2g^{-1}) and pore volume (0.5 cm^3 g^{-1}), and the pore diameter was not detected due to its non-porous property. Hence, this suggested that the mesostructured Cs-AlMCM-41 was not yet well established at this stage and this finding was supported by the XRD and TEM results.

The N_2 adsorption-desorption isotherm of the solids changed to type IV with distinct slit-shaped hysteresis loops when the heating time was extended (Figure 7b-d) where this revealed the presence of mesoporosity in the samples with slit-shaped pores (Kruk *et al.*, 1997). The samples (M-10h, M-14h and M-24h) showed remarkable increase in surface area, pore volume but slightly reduced in pore dimeter (Table 1, Figure 7). Cs-AlMCM-41 hollow nanospheres (M-24h) recorded the highest surface area (563 m^2 g^{-1}) and pore volume (1.327 cm^3g^{-1}) where their pore diameter was recorded to be 19.71 nm (Figure 8).

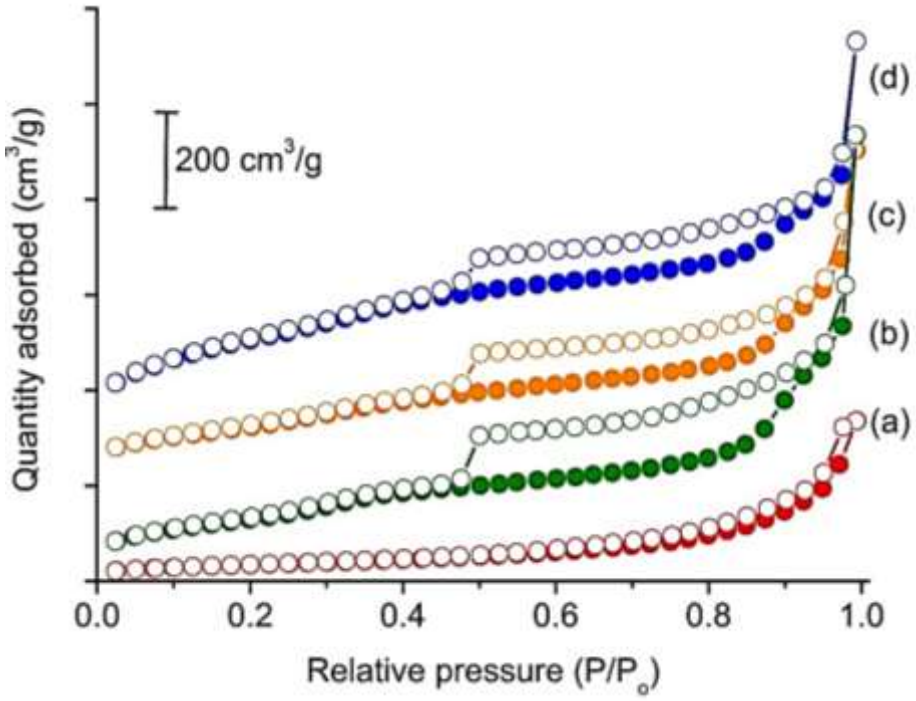

Figure 7. N_2 adsorption (close symbol) and desorption (open symbol) curves of (a) M-0h, (b) M-10h, (c) M-14h and (d) M-24h.

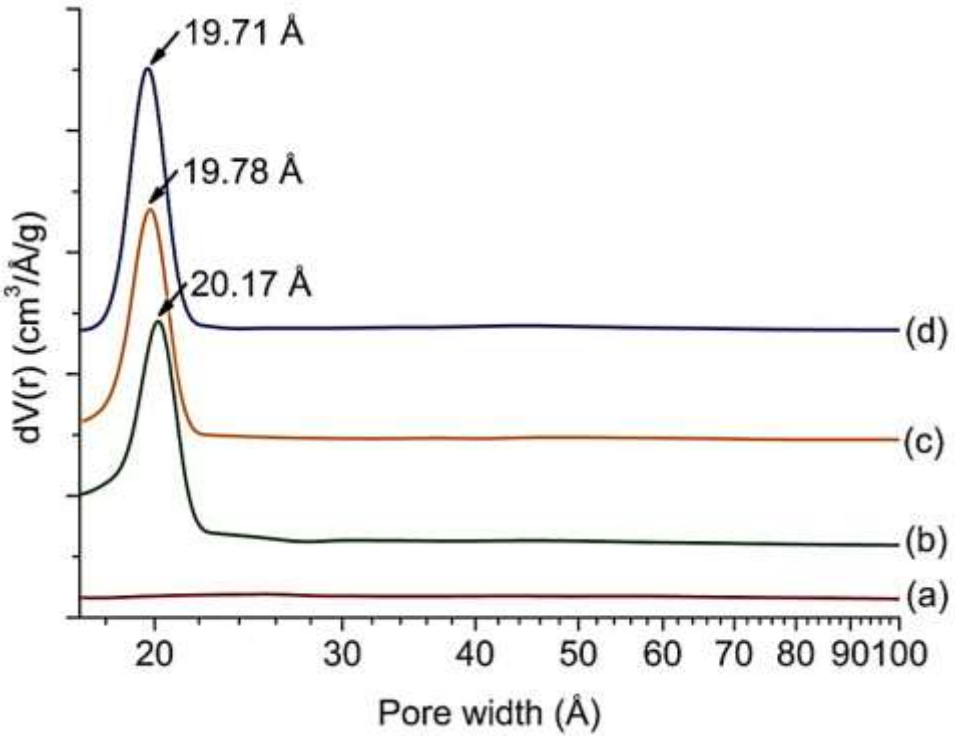

Figure 8. Pore size distribution of (a) M-0h, (b) M-10h, (c) M-14h and (d) M-24h.

The chemical composition of the samples was also determined using XRF spectroscopy analysis. As can be seen, the SiO_2/Al_2O_3 ratio of M-0h was 45.24, which was higher than that of the initial precursor solution (SiO_2/Al_2O_3 ratio = 30). When the hydrothermal treatment proceeded, the SiO_2/Al_2O_3 ratio continued to decrease indicating the active participation of Al into the amorphous samples. When the heating time was 10 h, the SiO_2/Al_2O_3 ratio of M-10h was 43.13. It decreased to 32.41 at 14 h before it further reduced to 30.11 after 24 h. In addition, the Cs was also found to actively participate in the formation of Cs-AlMCM-41 hollow nanospheres. At 0 h, the Cs_2O/Al_2O_3 ratio was very low which was merely 0.07. It increased to 0.38 after 10 h before it reached 0.52 after 24 h. In the formation of MCM-41, Cs serves as extra-framework cation to counterbalance the negative surface charge created by the isomorphous substitution of Al in the silicate framework structure (Ghear *et al.*, 2019).

Table 2: Chemical composition of samples heated at different times.

Samples	XRF spectroscopy analysis (%)				Cs_2O/Al_2O_3	SiO_2/Al_2O_3
	SO_2	Al_2O_3	Cs_2O	Others	molar ratio	molar ratio
M-0h	97.57	1.83	0.35	0.25	0.07	45.24
M-10h	95.52	2.02	2.13	0.33	0.38	43.13
M-14h	94.35	2.47	2.85	0.33	0.42	32.41
M-24h	93.32	2.63	3.79	0.26	0.52	30.11

CONCLUSION

The monitoring of the formation of cesium aluminosilicate (CsMCM-41) mesoporous material, under hydrothermal condition has been performed. The results demonstrated that when both surfactant, silica and alumina solutions were mixed under moderate stirring for 15 min, the process comprises homogenization of raw materials, where CTAB surfactants were first self-assembled into helical rod-like micelles, followed by hydrolysis, condensation and polymerization of silica and alumina precursors. After 0-16 h, the aluminosilicate oligomers which fully covered the helical cylindrical micelles underwent further condensation until completion. A well-defined and highly ordered CsMCM-41 which was thermally stable was obtained after 24 h of hydrothermal treatment. Thus, in summary, this study successfully gives a clear look on the formation of CsMCM-41 in cationic surfactant templated system. A clearer picture of the formation of CsMCM-41 has been obtained by observing the spectroscopy, microscopy and thermogravimetry data, which eventually leads us to a more comprehensive understanding of the self-assembly and chemical interactions in the surfactant system. Similar studies for other mesoporous materials under different conditions and approaches are encouraged since it may reveal more useful information for the understanding of the formation of mesostructured materials.

REFERENCES

Aiube, C.M., Oliveira, K.V.D. & Macedo, J.L.D. (2019). Effect of Cerium Precursor in the Synthesis of Ce-MCM-41 and in the Efficiency for Liquid-Phase Oxidation of Benzyl Alcohol. *Catalysts*, *9*(4), 377

Bagshaw, S.A. & Bruce, I.J. (2008). Rapid Calcination of High Quality Mesostructured MCM-41, MSU-X, and SBA-15 Silicate Materials: A Step Towards Continuous Processing? *Microporous and Mesoporous Materials*, *109*(1-3), 199-209.

Braga, P.R., Costa, A.A., de Macedo, J.L., Ghesti, G.F., de Souza, M.P., Dias, J.A. & Dias, S.C. (2011). Liquid phase calorimetric-adsorption analysis of Si-MCM-41: Evidence of strong hydrogen-bonding sites. *Microporous and Mesoporous Materials*, *139*(1-3), 74-80.

Ghrear, T.M.A., Rigolet, S., Daou, T.J., Mintova, S., Ling, T.C., Tan, S.H. & Ng, E.P. (2019). Synthesis of Cs-ABW Nanozeolite in Organotemplate-Free System. *Microporous and Mesoporous Materials*, *277*, 78-83.

Inagaki, S., Fukushima, Y. & Kuroda, K. (1993). Synthesis of Highly Ordered Mesoporous Materials from a Layered Polysilicate. *Journal of the Chemical Society, Chemical Communications*, (8), 680-682.

Jenkins, R. (2006). X-Ray Techniques: Overview. *Encyclopedia of Analytical Chemistry: Applications, Theory and Instrumentation*.

Kresge, C.T., Leonowicz, M.E., Roth, W.J., Vartuli, J.C. & Beck, J.S. (1992). Ordered Mesoporous Molecular Sieves Synthesized by a Liquid-Crystal Template Mechanism. *Nature*, *359*(6397), 710.

Kruk, M., Jaroniec, M. & Sayari, A. (1997). Adsorption Study of Surface and Structural Properties of MCM-41 Materials of Different Pore Sizes. *The Journal of Physical Chemistry B*, *101*(4), 583-589.

Liu H. & Xu P., (2019). Smart Mesoporous Silica Nanoparticles for Protein Delivery. *Nanomater. 9*, 1-23.

Liu X.Y., Tian B.Z., Yu C.Z, Gao F., Xie S.H., Tu B., Che R.C., Peng L.M., Zhao D.Y., Angew (2002). Periodic Mesoporous Organosilicas: Preparation, Properties and Application. *Chemical International Education, 41*, 3876-3878

Liu, Z.L., Yang, T.E.N.G., Zhang, K., Yan, C.A.O. & Pan, W.P. (2013). CO_2 Adsorption Properties and Thermal Stability of Different Amine-Impregnated MCM-41 Materials. *Journal of Fuel Chemistry and Technology*, *41*(4), 469-475

Matei, D., Cursaru, D.L. & Mihai, S. (2016). Preparation of MCM-48 Mesoporous Molecular Sieve Influence of Preparation Conditions on the Structural Properties. *Digest Journal of Nanomaterials and Biostructures*, *11*(1), 271-276.

Narayan, R., Nayak, U., Raichur, A. & Garg, S. (2018). Mesoporous Silica Nanoparticles: A Comprehensive Review on Synthesis and Recent Advances. *Pharmaceutics*, *10*(3), 118

Petcu, C., Purcar, V., Spătaru, C.I., Alexandrescu, E., Şomoghi, R., Trică, B. & Jecu, M.L. (2017). The Influence of New Hydrophobic Silica Nanoparticles on the Surface Properties of the Films Obtained from Bilayer Hybrids. *Nanomaterials*, *7*(2), 47.

Rahman, M.M., Aznan, M.A.B.M., Yusof, A.M., Ansary, R.H., Siddiqi, M.J. & Yusan, S. (2017). Synthesis and Characterization of Functionalized Se-MCM-41 a New Drug Carrier Mesopore Composite. *Oriental Journal of Chemistry*, *33*(2), 611.

Slowing, I., Trewyn, B.G. & Lin, V.S.Y. (2006). Effect of Surface Functionalization of MCM-41-Type Mesoporous Silica Nanoparticles on the Endocytosis by Human Cancer Cells. *Journal of the American Chemical Society*, *128*(46), 14792-14793.

Tanev, P.T. & Pinnavaia, T.J. (1995). A Neutral Templating Route to Mesoporous Molecular Sieves. *Science*, *267*(5199), 865-867.

Watanabe, R., Hagihara, H. & Sato, H. (2018). Structure-Property Relationships of Polypropylene-Based Nanocomposites Obtained by Dispersing Mesoporous Silica into Hydroxyl-Functionalized Polypropylene. Part 1: Toughness, Stiffness and Transparency. *Polymer Journal*, *50*(11), 1057

Yıldırım, Z.E., Gediz İliş, G., Mobedi, M. & Ülkü, S. (2011). Effect of Isotherm Shape on Mass Transfer in an Adsorbent Particle; An Isothermal Adsorption Process

Zhou, W. & Wang, Z.L. (Eds.). (2007). *Scanning Microscopy for Nanotechnology: Techniques and Applications*. Springer science & business media.